Available online at www.CivileJournal.org

Civil Engineering Journal

(E-ISSN: 2476-3055; ISSN: 2676-6957)

Vol. 11, No. 11, November, 2025

Numerical Analysis on Fatigue Performance in Fillet Weld Roots of Steel Bridge Bearings

Jiahao Mao [1], Feng Jiang [1], Mikihito Hirohata [1*], Yanyue Qin [2]

[1] Graduate School of Engineering, The University of Osaka, Suita, Osaka 565-0871, Japan.

[2] Department of Civil Engineering, The University of Tokyo, Bunkyo, Tokyo 113-8656, Japan.

Received 07 July 2025; Revised 19 October 2025; Accepted 23 October 2025; Published 01 November 2025

Abstract

Fillet weld roots near bridge supports are critical fatigue-prone details in steel bridges, particularly under high stress concentration. Fatigue cracks at these locations tend to be initiated internally, where detection and repair remain challenging with current techniques. Fatigue performance improvements are explored from the perspectives of structural design and epoxy insertion. Five actual bridges in the USA, China, and Japan were analyzed using a hybrid finite element modeling approach, employing low-precision girder models for load distribution and high-precision local support models with an introduced notch for Effective Notch Stress (ENS) evaluation. Both actual bridge case studies and numerical parametric analyses were conducted. Results indicate that increasing weld size effectively reduces ENS, while sole plate thickness has a limited effect. Bolts play a pivotal role in limiting relative displacement between the bottom flange and the sole plate, though their constraint range is localized. To address the limited effectiveness of structural adjustments, adhesive filling was introduced in areas beyond the bolt constraint range. Bonding-assisted welding with epoxy insertion achieved up to a 56% reduction in ENS and significantly improved fatigue performance. The findings confirm the potential of bonding-assisted welding for improving the durability of fillet weld roots in steel bridge supports and provide practical solutions to the difficult-to-detect root fatigue cracks.

Keywords: Steel Bridges; Fillet Welding; Fatigue; Structural Optimization; Bonding-Assisted Welding; Numerical Simulations.

1. Introduction

Bridges are essential infrastructures, enabling connectivity and supporting economic and social activities. Among the various types, steel bridges are often preferred, particularly in earthquake-prone regions, due to their lighter weight, higher ductility, superior seismic performance, and environmental benefits [1, 2]. These characteristics make steel bridges a reliable solution for ensuring safety and resilience under demanding conditions. Bridge bearings, as vital components of steel bridges, transfer loads and accommodate movements to maintain structural stability and longevity. Despite their essential role, these components are highly susceptible to fatigue-related damage due to high stress concentrations [3-5]. Such fatigue issues may compromise structural integrity, increase maintenance requirements, and pose safety risks. Addressing these challenges is crucial to enhancing the durability and reliability of bridge infrastructure.

Currently, it is common practice to connect the bottom flange, sole plate, and bearing using bolts [6, 7]. This construction method is simple and efficient. However, in bridge bearings subjected to large reaction forces, bolting alone is often insufficient to ensure structural strength and integrity. Consequently, a hybrid connection of bolting and welding

* Corresponding author: hirohata@civil.eng.osaka-u.ac.jp

http://dx.doi.org/10.28991/CEJ-2025-011-11-020

is typically adopted, where additional fillet welds are applied around the sole plate to connect it to the bottom flange of the girder, as illustrated in Figure 1. In highly corrosive environments, such as cross-sea bridges and port facilities, bolts are also prone to corrosion fatigue failure [8], making the hybrid connection a safer design. While numerous studies have focused on preventing surface fatigue cracks and have achieved notable results [9-12], research has shown that fatigue cracks also frequently initiate at the weld roots near bridge bearings, propagating from within the structure [4]. Unlike surface cracks, weld root cracks are difficult to detect using conventional inspection techniques and are challenging to repair even after being identified [13], which represents a significant drawback of welded connections in bridge bearings.

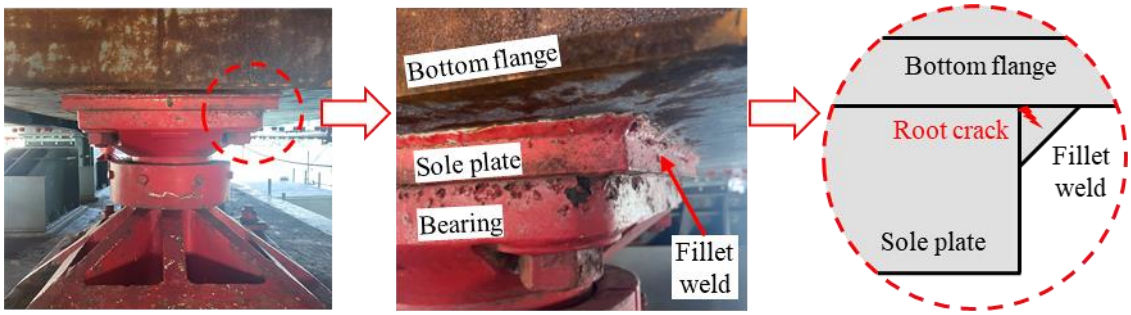

Figure 1. Connection details between the beam and bearing of a bridge

The fillet weld between the bottom flange and the sole plate near the bridge supports is a non-penetration weld, often leading to poor structural integrity between the two steel plates. This configuration presents a latent risk of fatigue cracks at the weld root. Addressing this issue requires innovative approaches to reduce stress concentration at the weld root during both design and construction. Niwa et al. proposed the use of tap bolts to prevent weld root cracking; however, this method involves drilling, which may compromise structural integrity [14]. Another promising solution is bonding-assisted welding technology, which inserts materials between the bottom flange and the sole plate [15, 16]. Previous experiments have demonstrated that inserting adhesive material such as epoxy resin or soft metal such as zinc between the bottom flange and the sole plate significantly improves their structural integrity [17, 18]. Furthermore, epoxy resin has also been used to bond steel plates when repairing fatigue cracks that originate from the weld roots of U-ribs in orthotropic bridge decks [19].

Despite the promising potential of epoxy-bonding-assisted welding in mitigating fatigue issues, its application in real-world bridge bearings remains insufficiently explored. This study aims to address this gap by evaluating the feasibility and effectiveness of the method through numerical analysis and actual bridge case studies. However, evaluating the fatigue life of weld roots is inherently challenging due to the structural complexity near bridge supports. The nominal stress method, commonly used for fatigue evaluation, performs poorly in such cases due to its inability to accurately capture stress concentrations [20, 21]. Similarly, the structural stress method encounters challenges in determining appropriate stress concentration factors [22, 23]. In addition, when using the finite element method to calculate weld root stress, the issue of stress singularity arises—an inevitable mathematical problem in finite element calculations. Stress singularity typically occurs at geometric discontinuities, such as weld roots and weld toes, where stress values are highly sensitive to element size and do not reflect actual fatigue stresses [24]. To overcome this, the Effective Notch Stress (ENS) method was developed. Based on the stress averaging theory, the ENS method alleviates stress singularities by introducing an artificial arc-shaped notch at the stress singularity. Fatigue performance is then evaluated using the stress value at this notch, providing an alternative and more accurate approach to fatigue evaluation [25-27].

Fillet welds between the bottom flange and the sole plate of bridges often feature complex geometries and are subjected to bending–shear coupling loads. However, the current IIW recommendations do not provide nominal stress-based evaluation methods for such welds [28]. In practice, most of these welds are still designed based on engineering experience, which may pose safety risks. Therefore, the fatigue life of the fillet weld root between the bottom flange and the sole plate is evaluated using the ENS method, and the applicability of this approach to bridge bearing analysis is examined. To improve computational efficiency, low-precision girder models are used to calculate the load, and high-precision local models of bridge support are employed to evaluate fatigue life at the weld root [29]. In addition, this study explores fatigue performance improvement strategies from both structural design and epoxy insertion perspectives. The overall research workflow is illustrated in Figure 2. By offering insights into practical implementation and performance, this research contributes to advancing fatigue prevention techniques and improving the design and maintenance of steel bridges, especially at critical locations such as the weld roots of bridge bearings.

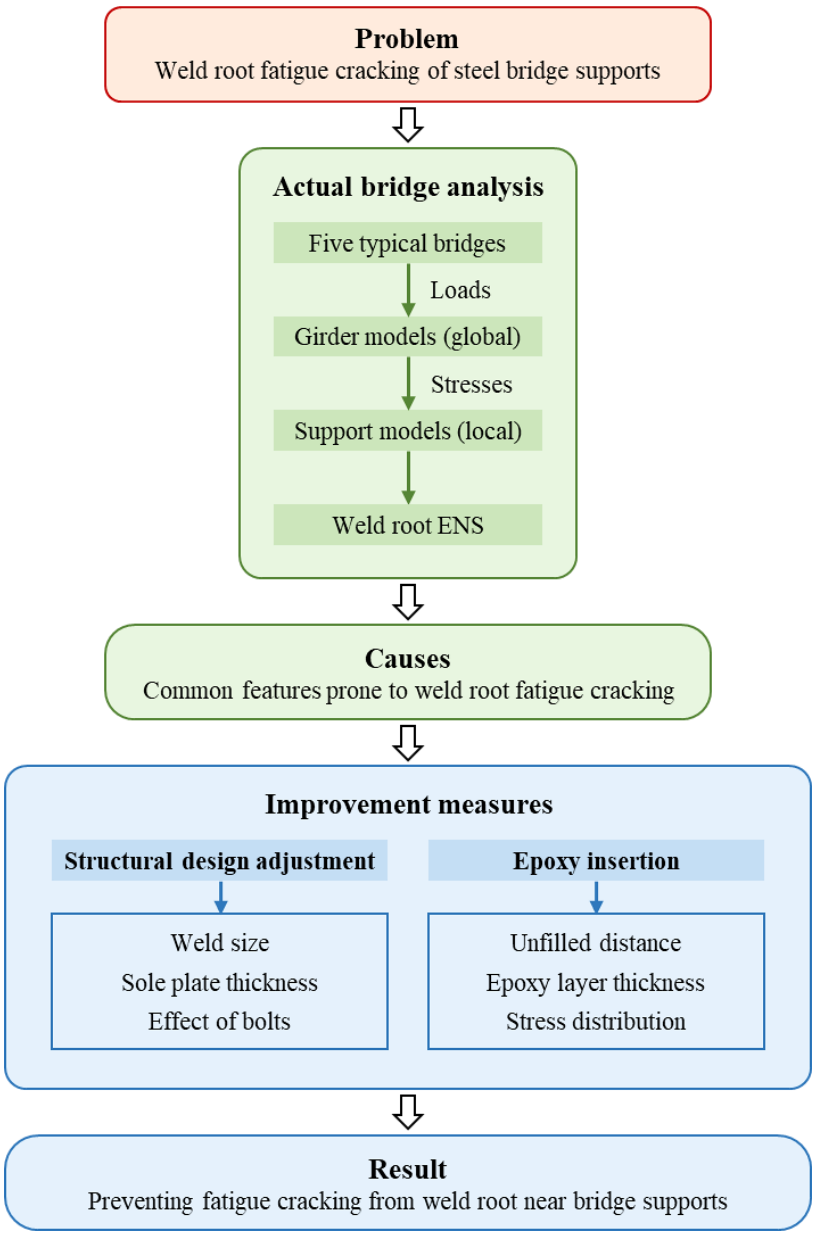

Figure 2. Overview of workflow

2. Bridge Information

To investigate the fatigue performance of fillet welds near bridge supports, five typical steel bridges or steel-concrete composite bridges in real-world were selected. Their basic information is summarized in Table 1. These bridges are located in the USA, China, and Japan. As shown in Figure 3, all bridges use I-section steel girders, with the number of girders ranging from 2 to 7. The structural details of the intermediate support cross-sections are provided in Table 2, and the detailed configurations near the supports, including size definitions, are illustrated in Figure 4. The bottom flange, sole plate, and bearing are connected using a combination of welding and bolting. Fillet welds are applied along the edge of the sole plate to connect it to the bottom flange.

Table 1. Basic information of selected bridges

Bridge ID	Bridge Type	Span design			Bridge width (m)	Number of girders
		Number	Length (m)	Total (m)		
C-1	Highway	3	30.0 + 36.0 + 30.0	96.0	14.20	6
C-2	Highway	3	48.9 + 41.0 + 53.9	143.8	10.14	2
C-3	Highway	4	4 × 20.0	80.0	14.00	7
C-4	Highway	5	34.9 + 3 × 38.0 + 34.9	183.8	14.75	3
C-5	Railway	3	30.0 + 40.0 + 30.0	100.0	1.70	2

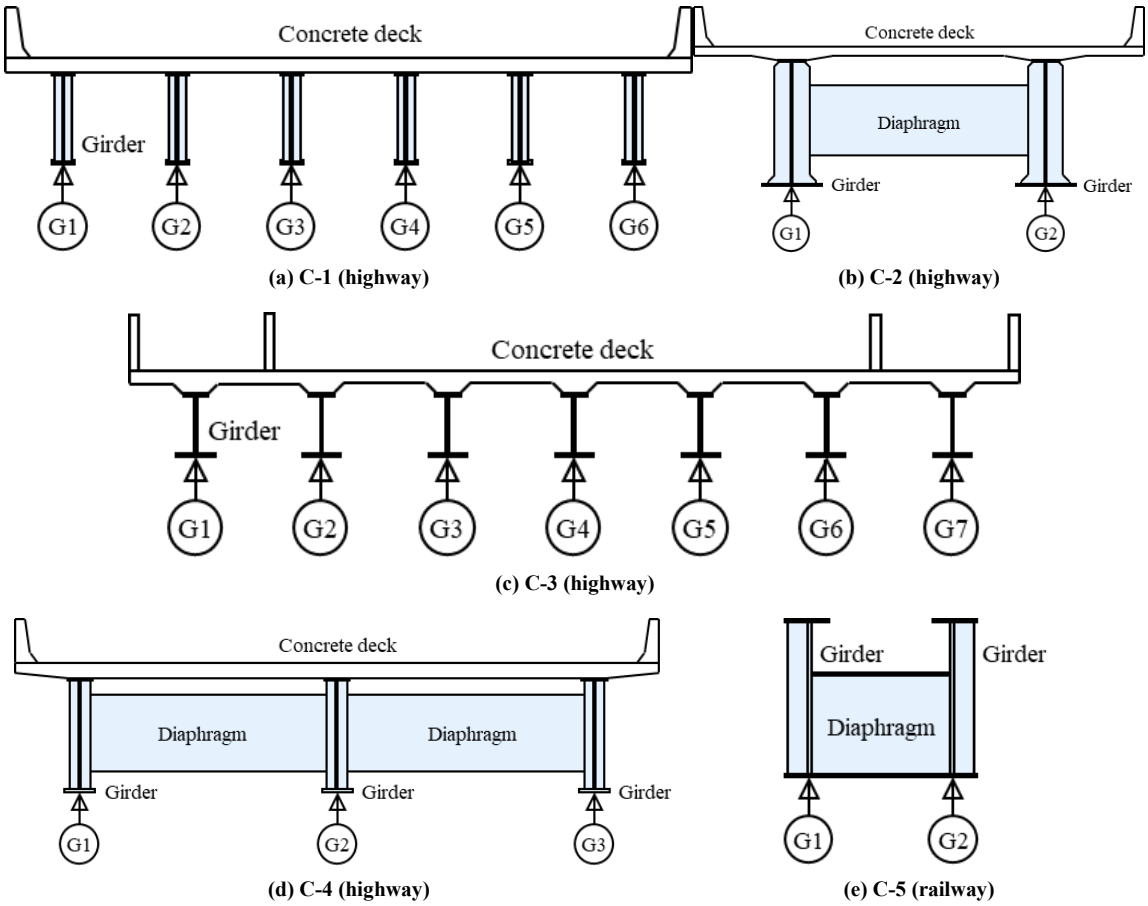

Figure 3. Cross-sections of selected bridges (unit: mm)

Table 2. Cross-sectional details at intermediate supports (unit: mm)

Bridge ID	Web		Bottom flange		Sole plate			Weld Leg
	Height h_w	Thickness t_w	Width $w_{b1}(w_{b2})$	Thickness t_b	Length l_s	Height h_w	Thickness t_w	Width $w_{b1}(w_{b2})$
C-1	1500	20	400	20	280	480	40	10
C-2	2800	20	870 (1350)	34	1370	1320	50	10
C-3	900	14	600	32	340	340	30	16
C-4	2200	12	620 (740)	35	700	700	39	10
C-5	1300	12	850 (1010)	22	1000	680	50	10

Note: Values in parentheses indicate the widened width of the bottom flange near the support.

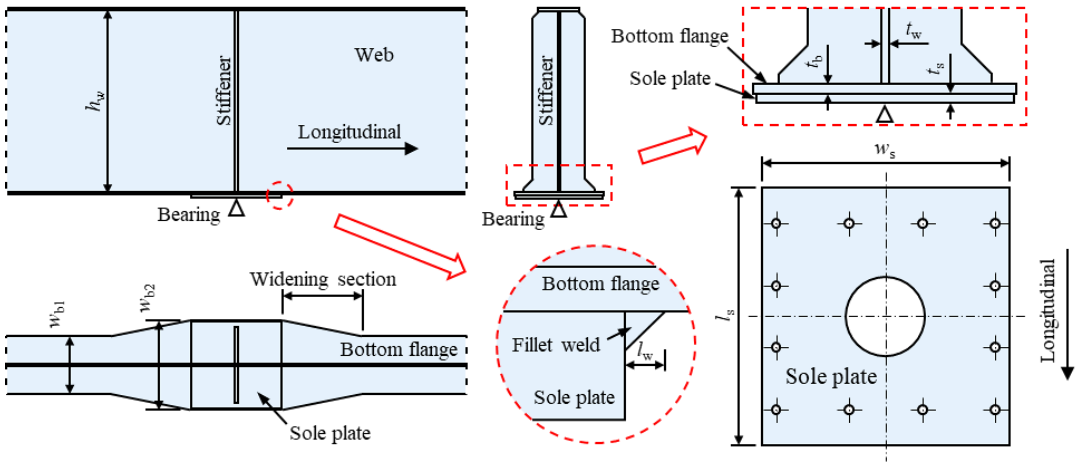

Figure 4. Structural details near the bridge supports

3. Fatigue Evaluation

Since this study focuses on the structural details at the weld root near bridge supports, a high-precision model is required for accurate analysis. However, creating a high-precision model for the entire bridge would be resource-intensive and computationally inefficient. Therefore, a combination of low-precision girder models and high-precision local support models was developed. Stress distributions near the supports were first obtained using the girder models. These loads were then applied to the high-precision local models to analyze the fatigue stress at the weld root. This hybrid modeling approach not only ensures computational efficiency but also achieves a high level of analytical accuracy.

3.1. Girder Models

The girder models are primarily used to analyze stress distributions near the supports. The five selected bridges have between 2 and 7 girders. To simplify the analysis, single-girder models were developed, and the applied loads were scaled by the number of girders, as illustrated in Figure 5. Load combinations were determined according to the relevant specifications for each bridge's country: *AASHTO LRFD Bridge Design Specifications* (USA) [30], JTG D60-2015 *General Specifications for Design of Highway Bridges and Culverts* (China) [31], TB 10002-2017 *Code for Design on Railway Bridge and Culvert* (China) [32] and *Specifications for Highway Bridges* (Japan) [33]. The fatigue load combination includes both the dead load and vehicle (or train) load, with load factors set to 1.0.

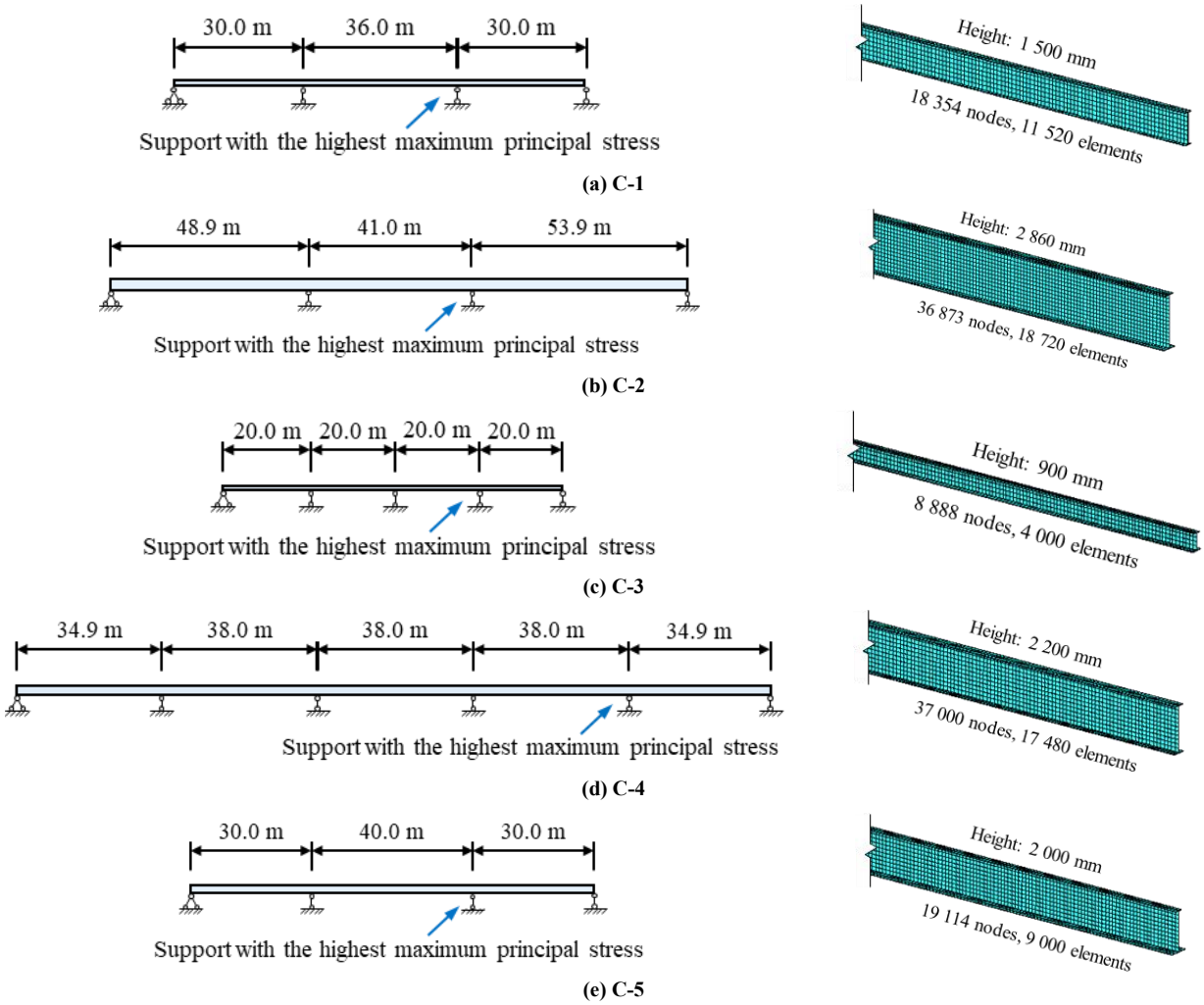

Figure 5. Girder models

Each model consists of 3D 8-node brick elements with reduced integration, with a global element size of 200 mm. The number of nodes and elements for each model is shown in Figure 5. The analysis focuses on the region near the intermediate support. To simplify the modeling process, the tensile contribution of concrete is neglected. These models include only the steel I-girder, while the concrete deck is represented as a uniformly distributed load applied to the upper flange. Diaphragms and stiffeners, as well as longitudinal slope, transverse slope, and curvature, are omitted for simplification. One edge of the girder is modeled as a pinned support, while the remaining supports are modeled as roller supports. All models are analyzed under linear elastic conditions, assuming an elastic modulus of 2.06×10^5 N/mm^2 and a Poisson's ratio of 0.3 for steel. Based on the fatigue load combinations, the support with the highest maximum principal stress in each bridge is selected for detailed analysis, and corresponding local support models are developed.

3.2. Support Models

3.2.1. Meshing Strategy

The structural configuration near the bridge support is highly complex, particularly at the fillet weld root between the bottom flange and the sole plate, where severe stress concentration occurs. As a result, the nominal stress method is unsuitable for evaluating the fatigue strength of the weld root in this context [17]. During finite element analysis, the calculated stress at the weld root is highly sensitive to the element size, a phenomenon commonly referred to as stress singularity. To address this, Radaj et al. introduced the concept of the ENS method, building on the microstructural support effect proposed by Radaj et al. [20]. This method artificially introduces a standard circular notch at the stress singularity to evaluate the fatigue strength of the weld based on the stress distribution around the notch. A commonly adopted practice is to use a circular notch with a reference radius of r_{ref} = 1 mm, as shown in Figure 6.

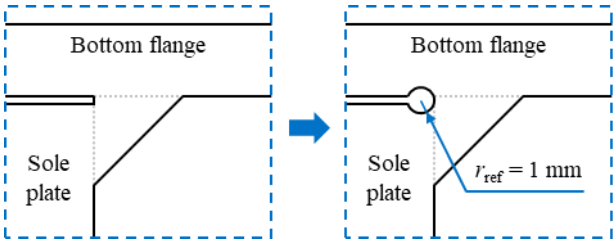

Figure 6. Structural details near the bridge supports

Multiple local finite element models of the bridge supports were developed using ABAQUS CAE 2018, using a modeling approach validated in previous studies by Jiahao et al. [17], and Mao et al. [18]. As shown in Figure 7, the support models include the local structure near the support of the girder, and a 1/2 model is constructed by symmetry. The support models also exclude the longitudinal slope, transverse slope, and curvature of the actual bridges. A notch with a reference radius r_{ref} of 1 mm was introduced at the fillet weld root between the bottom flange and the sole plate to facilitate ENS evaluation. The models use 3D 8-node brick elements with reduced integration (C3D8R). The element size along the notch perimeter is 0.2 mm, and the surrounding elements gradually transition to a global element size of 20 mm. All analyses are conducted under elastic conditions, with material properties identical to those of the girder models. The weld metal and base metal are assumed to have the same mechanical properties.

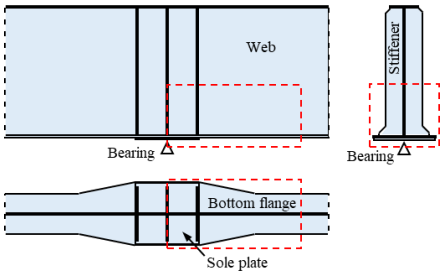

(a) Position of the support models

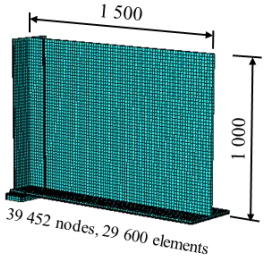

(b) C-1

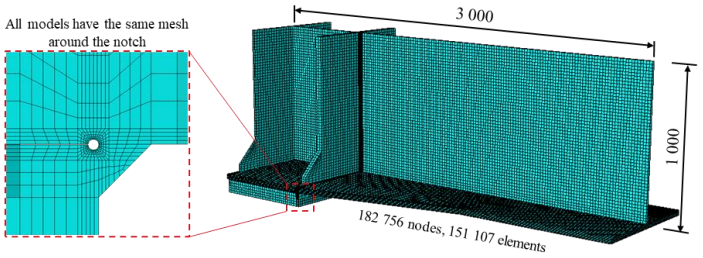

(c) C-2

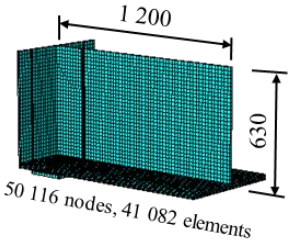

(d) C-3

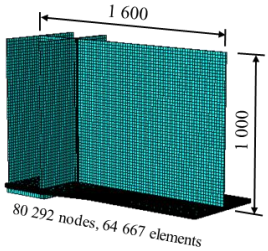

(e) C-4

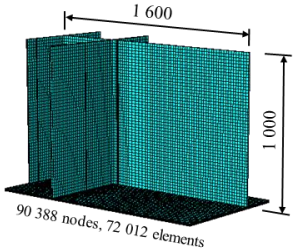

(f) C-5

Figure 7. Support models

3.2.2. Boundaries and Loads

The boundary and loading conditions for the support models are illustrated in Figure 8. A symmetric boundary condition is applied along the mid-axis cross-section of the support, while a pin support is assigned to the sole plate. Both normal and shear loads are simplified as linearly varying distributed loads applied on the cut surfaces of the support model. These loads are derived from the stress distribution at the support with the highest maximum principal stress in the girder models, and are expressed as follows:

$$N_x(y) = k_1 y + \sigma_1 \quad (1)$$

$$N_y(x) = k_2 x + \sigma_2 \quad (2)$$

$$S_{xy}(y) = k_3 y + \tau_1 \quad (3)$$

$$S_{yx}(x) = k_4 x + \tau_2 \quad (4)$$

where, $N_x(y)$, $N_y(x)$, $S_{xy}(y)$ and $S_{yx}(x)$ represent the distributed normal and shear loads in the *x*- and *y*-directions, respectively. The coefficients k_1, k_2, k_3, k_4, σ_1, σ_2, τ_1 and τ_2 are load constants obtained from the girder models, as summarized in Table 3.

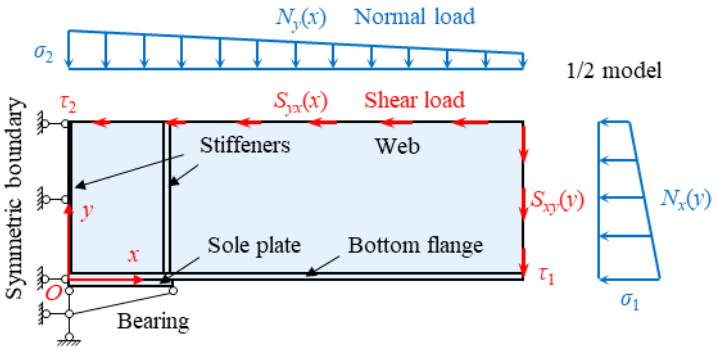

Figure 8. Boundary and loading conditions for the support models

Table 3. Values of load constants

Bridge ID	$N_x(y)$		$N_y(x)$		$S_{xy}(y)$		$S_{yx}(x)$	
	k_1	σ_1	k_2	σ_2	k_3	τ_1	k_4	τ_2
C-1	0.0719	-54.172	0.0024	-1.600	-0.0059	0.0719	-54.172	0.0024
C-2	0.0401	-51.858	0.0133	-30.561	-0.0151	0.0401	-51.858	0.0133
C-3	0.0941	-27.998	0.0076	-7.893	-0.0167	0.0941	-27.998	0.0076
C-4	0.0514	-60.092	0.0269	-39.122	-0.0195	0.0514	-60.092	0.0269
C-5	0.0562	-50.747	0.0184	-26.016	-0.0144	0.0562	-50.747	0.0184

3.2.3. Simulation of Bolts

No solid elements are introduced to model the bolts. Instead, their effect is simulated using displacement constraint equations between paired nodes, as illustrated in Figure 9. The bolt preload is neglected. Bolts are assumed to restrict the relative displacement between the bottom flange and the sole plate. The relative displacement vector $\vec{d}$ is defined as:

$$\vec{d} = \vec{d}_A - \vec{d}_B \quad (5)$$

where; $\vec{d}_A$ and $\vec{d}_B$ are the displacements of the paired nodes on the bottom flange and the sole plate, respectively, as expressed in the following Equations:

$$\vec{d}_A = (u_A, v_A, w_A) \quad (6)$$

$$\vec{d}_B = (u_B, v_B, w_B) \quad (7)$$

where; u_A, v_A and w_A are the displacement components of $\vec{d}_A$ in the *x*-, *y*- and *z*-directions, respectively; u_B, v_B and w_B are the corresponding components of $\vec{d}_B$.

Bolt constraints are divided into normal and tangential components. In the normal direction, bolts provide tension-only constraints and allow compressive deformation. In ABAQUS, "hard" contact is defined at the interface between the bottom flange and the sole plate to prevent element penetration under compression. In the tangential directions, bolts are modeled as providing rigid constraints, completely preventing relative movement between the nodes. The bolt constraint conditions can be summarized as:

$$\begin{cases} u_A - u_B = 0 \\ v_A - v_B \leq 0 \\ w_A - w_B = 0 \end{cases} \tag{8}$$

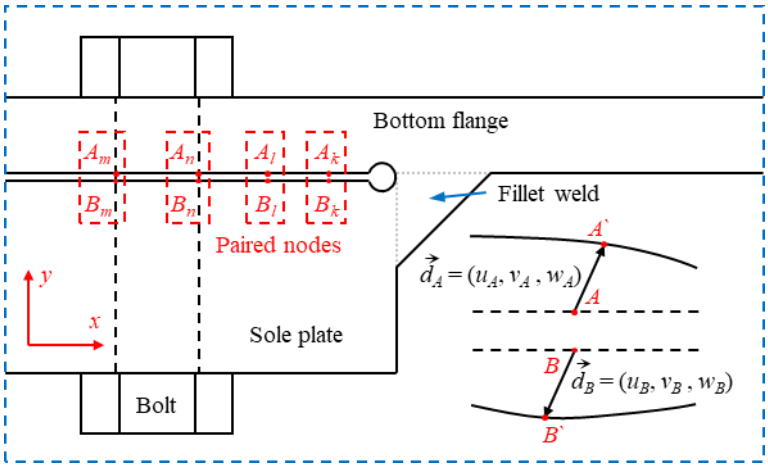

Figure 9. Relative displacement between paired nodes

3.3. Effective notch stress

Based on the local finite element models of the intermediate supports, the ENS at the fillet weld root between the bottom flange and the sole plate was analyzed for five bridges. Welding-induced residual stresses and welding sequence were not considered in the analysis. The fatigue life of the weld root was evaluated using the FAT 225 design curve, following the *Recommendations for fatigue design of welded joints and components* from IIW Collection [28]. The ENS values and corresponding fatigue life predictions are shown in Figure 10. Among the five bridges, only C-3 exhibited a low ENS of 127.8 N/mm^2, whereas three bridges showed ENS values exceeding 225 N/mm^2, indicating a predicted fatigue life of less than 2 million cycles. Notably, C-2 and C-4 exhibited particularly high ENS values—331.7 N/mm^2 and 275.9 N/mm^2, respectively—corresponding to predicted fatigue lives of only 6.24×10^5 and 10.85×10^5 cycles, respectively. Given that both C-2 and C-4 are highway bridges, the risk of fatigue cracking at the weld root is significant under heavy traffic conditions, potentially increasing long-term maintenance costs.

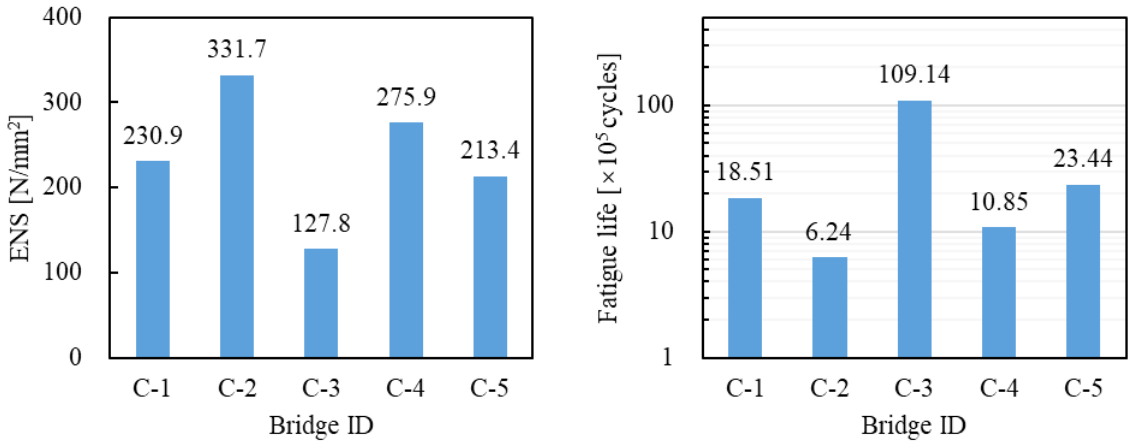

(a) ENS **(b) Predicted fatigue life**

Figure 10. Results of weld root fatigue evaluation

It is worth noting that the deck widths and live loads of the four highway bridges (C-1 to C-4) are similar, yet the ENS values of C-1 (6 girders) and C-3 (7 girders), both employing multiple small girders, are substantially lower than those of C-2 (2 girders) and C-4 (3 girders). Furthermore, the ENS of C-2 is approximately 20% higher than that of C-

4. Although large-girder designs simplify construction and maintenance, they result in greater loads per support, thereby increasing the tensile stress at the weld root and reducing fatigue life. Hence, special attention should be given to weld root fatigue when adopting such designs. Comparing C-1 and C-3, although the number of girders differs only slightly, C-3 exhibits an ENS nearly half that of C-1. The main structural difference lies in weld size, with weld leg lengths of 10 mm in C-1 and 16 mm in C-3. The influence of weld size on fatigue performance is further discussed in Section 4.1.1. For the railway bridge C-5, although its dead load is significantly lower than that of the highway bridges, its live load is higher and constitutes a larger proportion of the total load. As a result, the ENS at its weld root is also relatively high, and fatigue cracks at the weld root between the bottom flange and the sole plate must be considered during service.

4. Parameter Analyses

Fatigue risks have been identified at the fillet weld root between the bottom flange and the sole plate in multiple bridges. To address this issue, this study investigates strategies to improve the fatigue life of the weld root through structural design optimization and epoxy insertion, based on parameter analyses. Among the five bridges previously evaluated, C-2 exhibited the highest ENS and the shortest predicted fatigue life. Therefore, C-2 was selected as the primary case for the subsequent parameter analyses.

4.1. Structural Design

Girder design typically prioritizes load-bearing capacity, making it impractical to modify the overall girder configuration solely to enhance the fatigue performance of the weld root near the bridge support. A more feasible approach is to optimize the design of the welds and sole plate. The comparative investigation of five actual bridges revealed that weld size may significantly influence the fatigue life of the weld root. Additionally, considerable variation in sole plate thickness was observed among the five selected bridges, and the ratio of sole plate thickness to bottom flange thickness may affect the relative stiffness, thereby influencing stress at the weld root. Accordingly, this section examines the influences of the fillet weld leg length l_w and sole plate thickness t_s on weld root fatigue performance. In addition, the effect of bolts on the ENS at weld root in hybrid connection of bolting and welding is also analyzed. The definitions of the relevant structural parameters are illustrated in Figure 11.

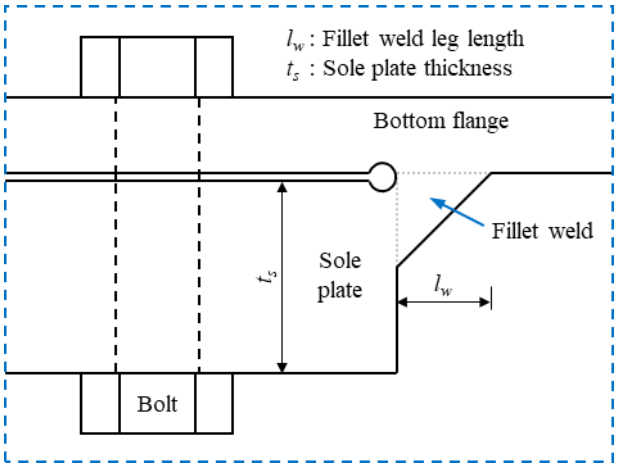

Figure 11. Structural parameters

4.1.1. Weld Size

Based on the bridge support design of C-2, the weld size was varied in the models by adjusting the fillet weld leg length l_w as a parameter. The actual design specifies a weld leg length of 10 mm, and a variation range from 6 mm to 20 mm was considered. The calculated ENS at the weld root and corresponding fatigue life predictions are shown in Figure 12. The ENS decreases as the weld leg length l_w increases. When l_w reaches 20 mm, the ENS is reduced to 227.1 N/mm^2, which is approximately 68% of the value under the original design. Although the predicted fatigue life is tripled compared to the baseline, it still falls short of 2 million cycles. However, increasing weld size as a means of improving fatigue life has limitations. First, the improvement effect diminishes with larger welds. Second, an excessively large weld makes single-pass welding impractical, complicates quality control, and increases construction difficulty and cost. These findings indicate that although increasing weld size can enhance fatigue performance, its application is constrained by construction feasibility. Therefore, increasing weld size can be regarded as an auxiliary rather than a primary measure for enhancing weld root fatigue life. Because for bridge details where weld root fatigue life is already insufficient, merely enlarging the weld size may not be sufficient to prevent fatigue cracks over the service life.

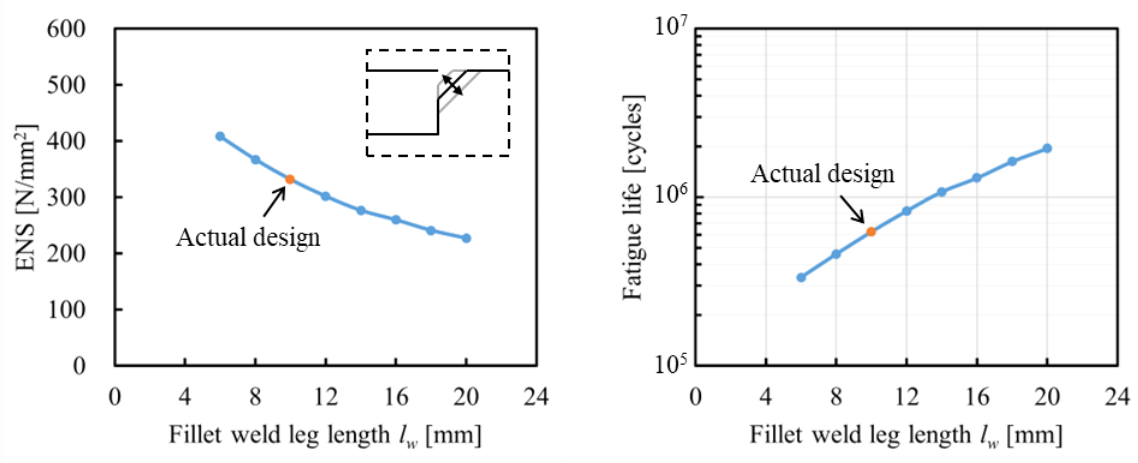

(a) ENS **(b) Predicted fatigue life**

Figure 12. Effect of weld size

4.1.2. Sole Plate Thickness

The influence of sole plate thickness t_s on the ENS and predicted fatigue life at the weld root is shown in Figure 13. The thickness was varied from 30 mm to 100 mm, while the actual bridge design uses a thickness of 50 mm. Although increasing the sole plate thickness slightly reduces the ENS, the overall effect is minimal. Even with an increase from 30 mm to 100 mm, the ENS decreases by less than 2%, and the fatigue life improves by less than 6%. These results indicate that increasing the sole plate thickness has limited effectiveness in enhancing the fatigue life of the weld root. Increasing the sole plate thickness primarily enhances its bending stiffness, thereby restricting deformation and reducing relative displacement between the bottom flange and the sole plate. The relative displacement can be decomposed into normal and tangential components. Since the bottom flange is typically thinner and much longer than the sole plate, the normal relative displacement mainly results from the deformation of the bottom flange, rendering the increase in sole plate thickness minimally beneficial. Furthermore, tangential displacement is governed by shear stiffness, which is only slightly affected by plate thickness. Hence, the effect of t_s on weld root fatigue life is minimal. Consequently, the sole plate thickness can be adjusted rationally to satisfy structural design requirements without significantly influencing the fatigue performance at the weld root.

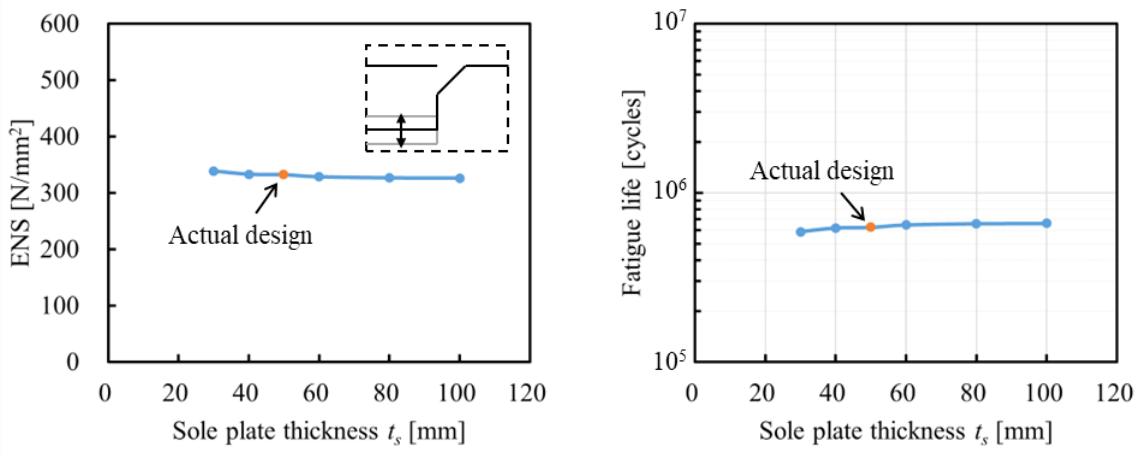

(a) ENS **(b) Predicted fatigue life**

Figure 13. Effect of sole plate thickness

4.1.3. Effect of Bolts

The weld root fatigue evaluations for the five bridges, including and excluding the effect of bolts (hybrid and welding), are presented in Figure 14. Compared to the hybrid connection of bolting and welding, models using welding alone showed increased ENS at the weld root across all five bridges, with increases ranging from 2% to 26%. This rise in ENS led to a corresponding reduction in predicted fatigue life. Bolts play a critical role in limiting the relative displacement between the bottom flange and the sole plate, thereby lowering ENS and enhancing fatigue performance of weld root. In particular, bridges C-2, C-4, and C-5 have substantially larger sole plates than C-1 and C-3, resulting in larger gaps and greater relative displacement. Consequently, bolts are especially effective in reducing ENS in these cases.

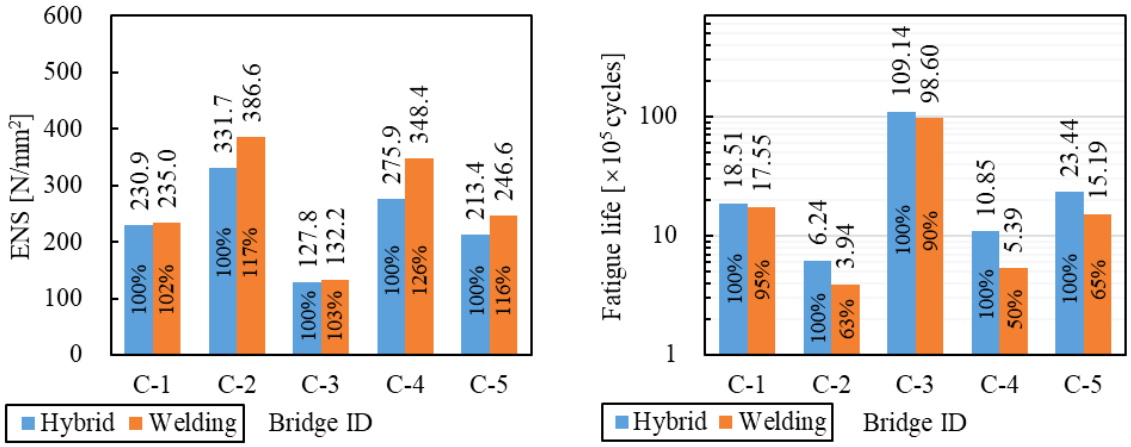

(a) ENS **(b) Predicted fatigue life**

Figure 14. Comparison of results with and without bolts

Taking C-2 as an example, the relative displacement between the bottom flange and the sole plate is plotted in Figure 15. In the hybrid connection model, the relative displacement is significantly reduced near the bolt locations. When comparing the hybrid connection with the welding-only model, the overall displacement is consistently smaller in the hybrid case. This confirms that bolts effectively restrain relative movement and reduce weld root ENS. However, it is worth noting that the constraint range of the bolts is limited. Beyond a 50 mm distance from a bolt, the difference in displacement between the two models becomes relatively small. Therefore, increasing the number of conventional bolts or placing them closer to the weld root is not a practical solution due to the required safety clearances from the edge of the sole plate. Therefore, Niwa et al. proposed installing tap bolts closer to the weld root. Because tap bolts are smaller than conventional bolts used for connecting the sole plate to the bottom flange, they can be placed more densely and nearer to the weld root, increasing the weld root fatigue life by approximately eightfold (after conversion) [14]. However, this method still requires drilling into the structure, which may compromise the integrity of the original components.

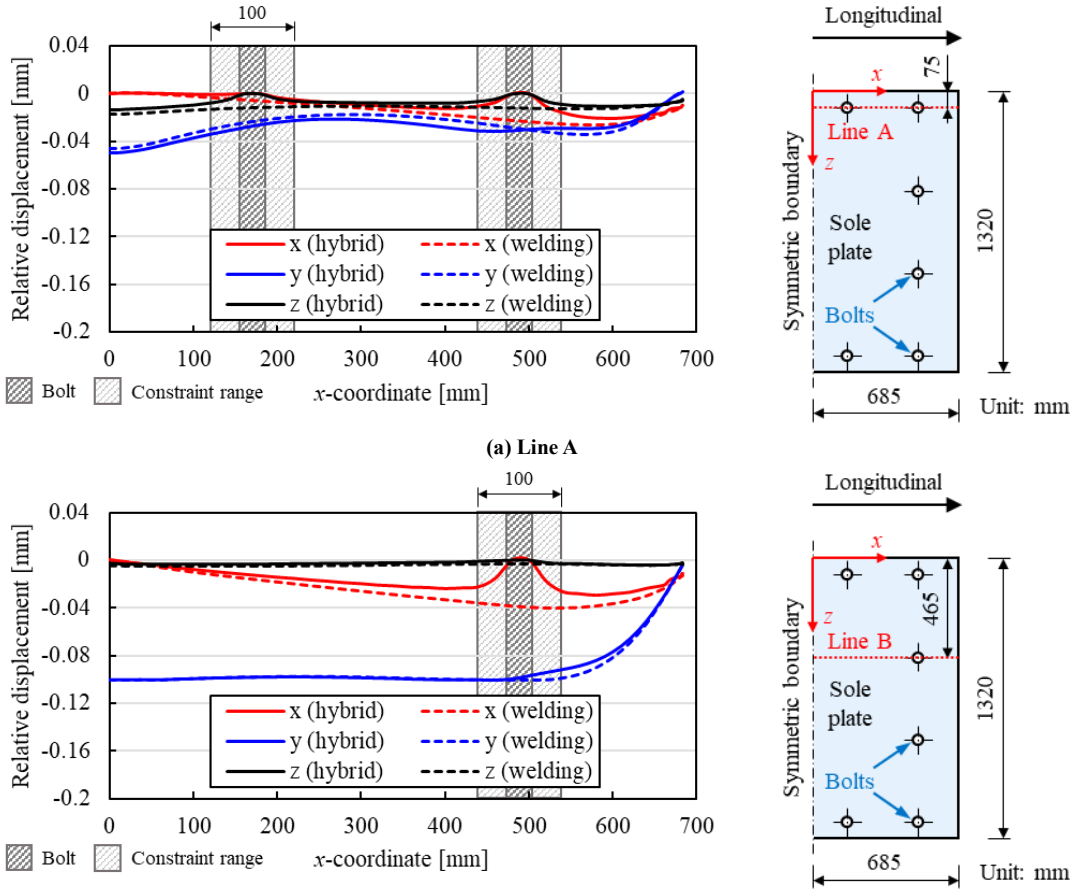

(a) Line A

(b) Line B

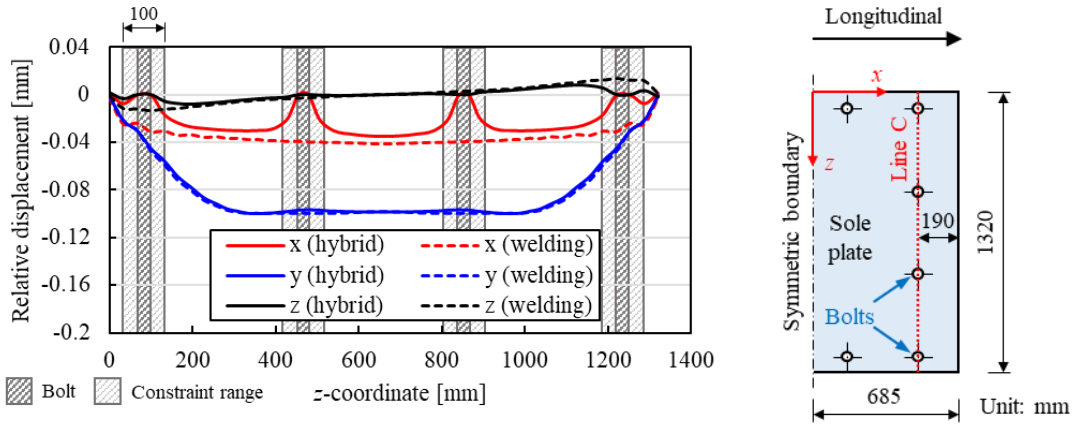

(c) Line C

Figure 15. Relative displacement between the bottom flange and the sole plate in C-2

This limitation motivates the use of bonding-assisted welding. In this method, adhesive material is inserted between the bottom flange and the sole plate to provide continuous bonding. It effectively restricts relative displacement over a wider area, reduces ENS, and improves the fatigue life of the weld root. The optimization of bonding-assisted welding is discussed in Section 4.2.

4.2. Epoxy Insertion

Although optimizing structural design can reduce the ENS at the weld root near bridge supports to some extent, it remains difficult to completely prevent fatigue cracks in certain bridges over their service life. To address this, epoxy resin is introduced as an adhesive material to bond the bottom flange and the sole plate, aiming to further reduce the weld root ENS and improve fatigue life. The effectiveness of bonding-assisted welding in enhancing weld root fatigue performance has been validated through model experiments [17, 18]. To optimize the application of this method in actual bridge structures, a series of numerical simulations was conducted. Two types of local support models were used: conventional welding (W) models and bonding-assisted welding (WB) models. Figure 16 illustrates the differences between the two models. The W model replicates the structural details and dimensions of the actual bridge, except for including a notch at the weld root. In the WB model, a groove of suitable thickness is cut into the sole plate to accommodate the epoxy layer and prevent burning during welding. The epoxy is assigned an elastic modulus of 3.8×10^3 N/mm^2 and a Poisson's ratio of 0.35, as reported in a previous study by Jiahao et al. [17]. The effects of three key parameters are examined in detail: the unfilled distance from the weld root to the epoxy layer d, the epoxy layer thickness t_e, and material strength of the epoxy. The definitions of unfilled distance d and thickness t_e are shown in Figure 16.

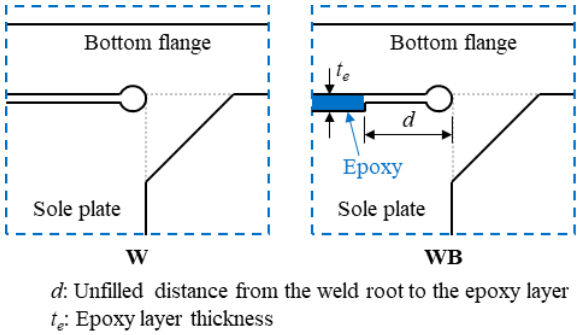

Figure 16. Differences between W and WB models

4.2.1. Unfilled Distance

To prevent the epoxy from burning during welding and causing defects, a safety distance must be maintained between the weld root and the epoxy. In this analysis, the unfilled distance from weld root to epoxy d varied from 10 mm to 80 mm, with the epoxy layer thickness t_e fixed at 0.50 mm. The results are presented in Figure 17. As shown in Figure 17-a, the ENS at the weld root increases as d increases. Compared to the W model, the WB model reduces ENS by 62% when d = 10 mm, and by 15% when d = 80 mm, indicating that the epoxy's constraint effect between the bottom flange and sole plate diminishes as the unfilled distance increases. Figure 17-b demonstrates that incorporating epoxy significantly improves fatigue life when the unfilled distance is small. At d = 80 mm, the fatigue

life of the WB model is 9.46×10^5 cycles, about 1.5 times that of the W model. But for d = 10 mm, the WB model achieves a fatigue life of 1.10×10^7 cycles, approximately 17.6 times greater than that of the W model. To ensure a fatigue life exceeding 2×10^6 cycles, the unfilled distance d should not exceed 40 mm. Figure 17-c shows the relationship between the maximum principal tensile stress in the epoxy layer $\sigma_{1,max}$ and d for WB models. When $d \leq$ 40 mm, $\sigma_{1,max}$ increases with d, rising from $\sigma_{1,max}$ = 18.6 N/mm^2 at d = 10 mm to $\sigma_{1,max}$ = 28.2 N/mm^2 at d = 40 mm. Beyond d = 40 mm, $\sigma_{1,max}$ stabilizes at approximately 24 N/mm^2. The reasons for this trend will be further discussed in Section 4.2.3.

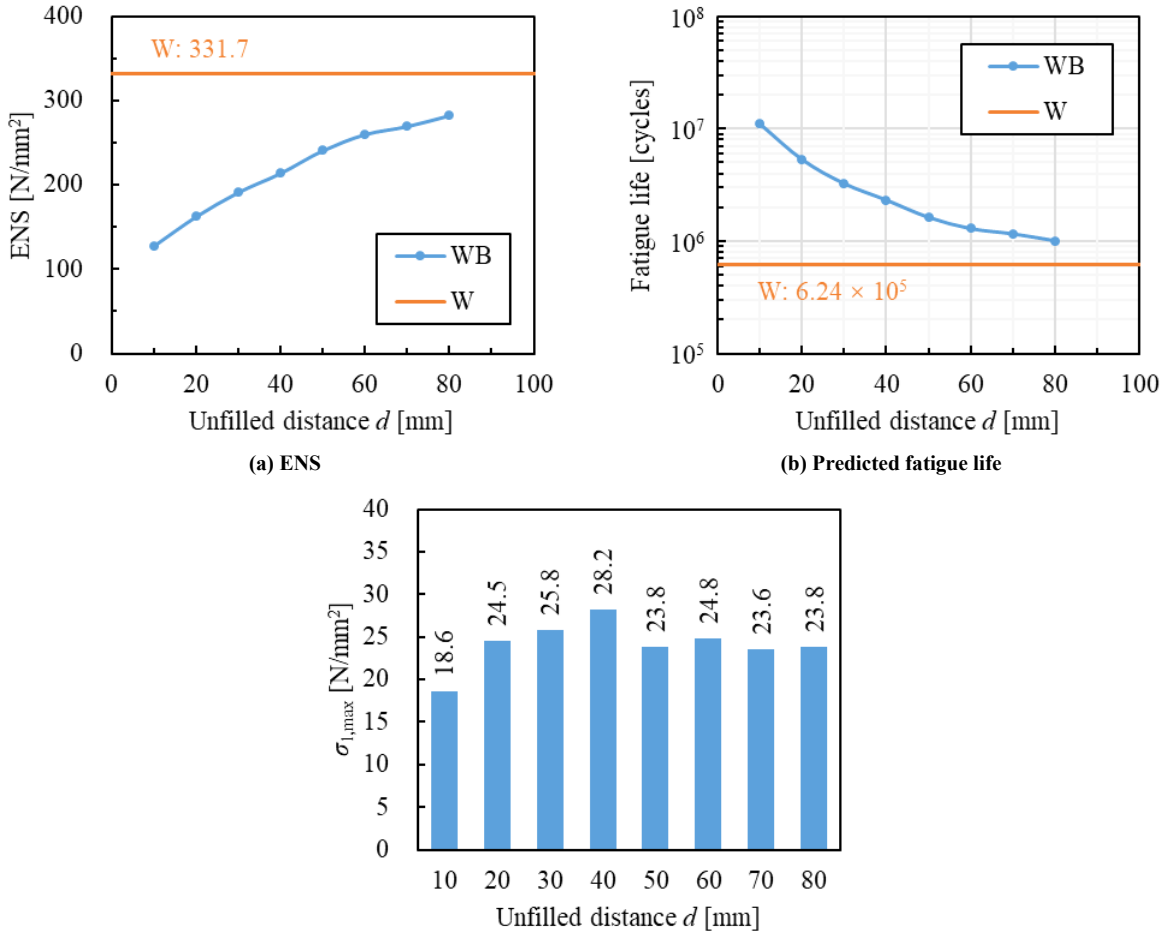

(a) ENS

(b) Predicted fatigue life

(c) Maximum principal tensile stress in epoxy

Figure 17. Effect of unfilled distance from weld root to epoxy

Therefore, the unfilled distance d should be minimized and preferably kept below 40 mm to substantially enhance weld root fatigue life and reduce stress in the epoxy layer. Previous studies recommended a minimum safety distance of $d \geq$ 15 mm to avoid burning the epoxy during welding. If necessary, finite element simulations of the welding process can be used to refine this distance. Additionally, surrounding the epoxy with heat-resistant rubber can help mitigate burning risks [17]. Even when maintaining a safety distance from 15 mm to 40 mm, epoxy insertion can reduce weld root ENS to as low as 45% of the original structure, while extending the fatigue life by more than tenfold. This required distance is considerably smaller than the edge clearances mandated for conventional bolt holes in the sole plate, allowing the epoxy to effectively constrain the relative displacement between the bottom flange and the sole plate, thereby enhancing weld root fatigue performance. The improvement achieved through epoxy insertion is significantly greater than that attainable by structural design modifications alone, demonstrating the strong potential of bonding-assisted welding for application in bridge supports.

4.2.2. Epoxy Layer Thickness

The influence of epoxy thickness t_e was analyzed up to 1.50 mm in increments of 0.25 mm, while maintaining a constant unfilled distance d of 20 mm across all models. The results are presented in Figure 18. All WB models demonstrated significant reductions in weld root ENS. The ENS increased as t_e grew. Depending on t_e, ENS was reduced by 39% to 66% relative to the W model. This trend is attributed to the lower elastic modulus of epoxy compared to steel,

as a thicker epoxy layer weakens the constraint effect between the bottom flange and sole plate. At t_e = 0.25 mm, the predicted fatigue life increased to 7.17 × 10^6 cycles, which is more than 11 times greater than that of the W model. Even at t_e = 1.50 mm, a value that exceeds common engineering practice, the fatigue life reached 2.69 × 10^6 cycles, which is four times the original design. The relationship between the maximum principal tensile stress in the epoxy $\sigma_{1,max}$ and the epoxy thickness t_e is shown in Figure 18-c. As t_e increases, $\sigma_{1,max}$ decreases, particularly when t_e is small. For instance, increasing t_e from 0.25 mm to 0.75 mm reduces $\sigma_{1,max}$ by approximately 42%, from 33.9 N/mm^2 to 19.6 N/mm^2. However, a further increase from 1.00 mm to 1.50 mm results in only a 20% reduction, from 16.6 N/mm^2 to 13.3 N/mm^2, indicating diminishing returns.

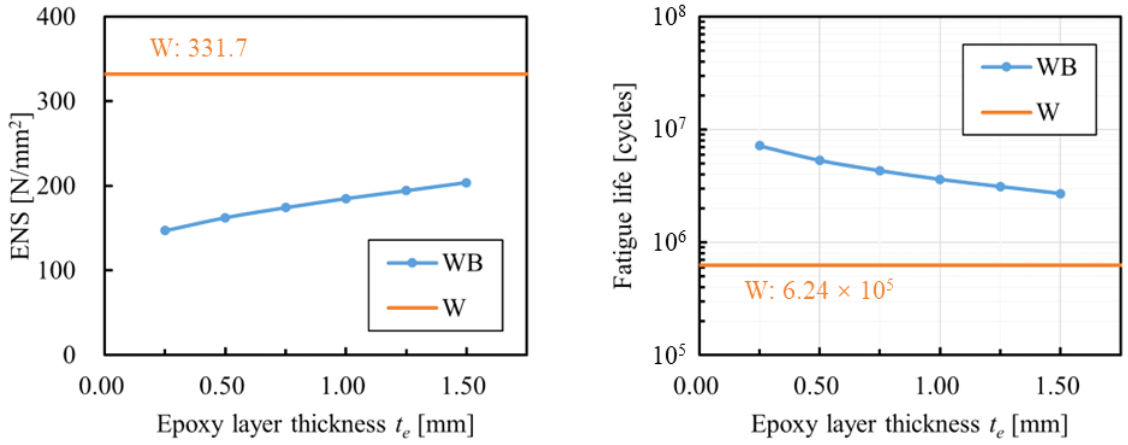

(a) ENS **(b) Predicted fatigue life**

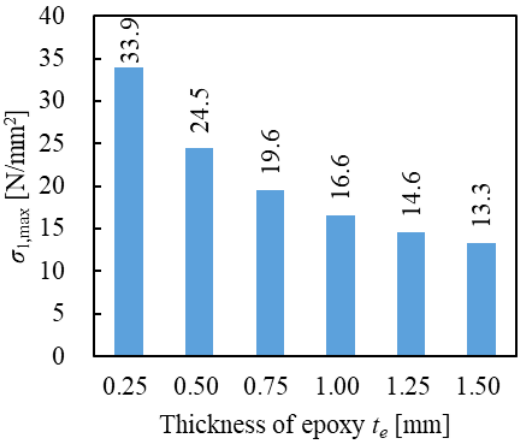

(c) Maximum principal tensile stress in epoxy

Figure 18. Effect of epoxy layer thickness

For practical applications, an epoxy layer thickness t_e between 0.50 mm and 1.00 mm is recommended. This range ensures a notable improvement in weld root fatigue life while effectively limiting stress in the epoxy layer. Prolonged exposure to high stress may negatively affect the epoxy's durability due to aging and fatigue [34].

4.2.3. Stress Distribution

In the above analysis, the maximum principal tensile stress in the epoxy layer showed relatively high values in some cases, which may lead to the risk of failure in practical applications. In addition, when discussing the relationship between the maximum principal tensile stress in the epoxy $\sigma_{1,max}$ and the unfilled distance d, it was found that the two are not monotonically positively or negatively correlated. Therefore, it is necessary to further analyze the stress distribution of epoxy. In engineering practice, the strength of epoxy is typically evaluated based on axial tensile strength and shear strength; hence, both aspects are examined here. Figures 19 and 20 present the variation of stress components with respect to the unfilled distance d and epoxy layer thickness t_e, respectively. The stress components include normal stress σ_y, shear stress τ_{xy} and τ_{yz}, and their corresponding maximum values are $\sigma_{y,max}$, $\tau_{xy,max}$ and $\tau_{yz,max}$, respectively. Figures 21 to 23 illustrate the stress distribution within the epoxy layer for d = 10 mm, 40 mm and 80 mm, respectively, with t_e = 0.50 mm.

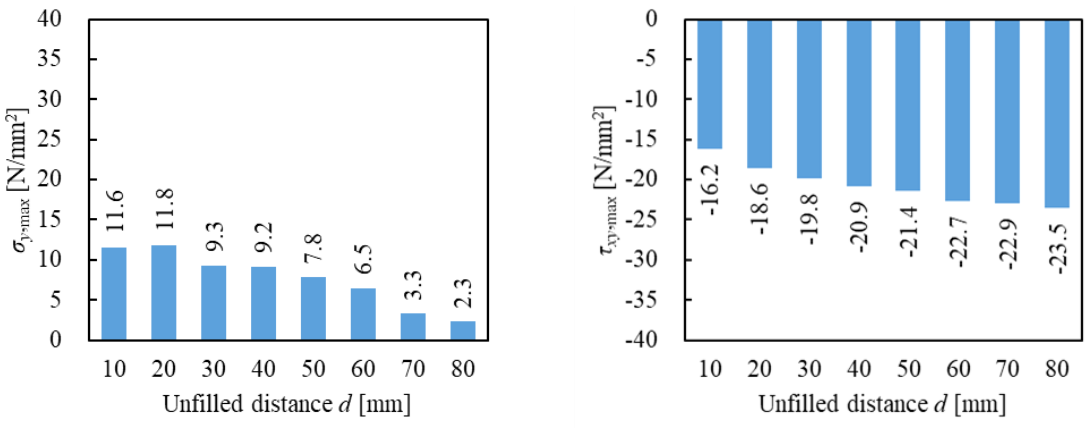

(a) Normal stress σ_y **(b) Shear stress τ_{xy}**

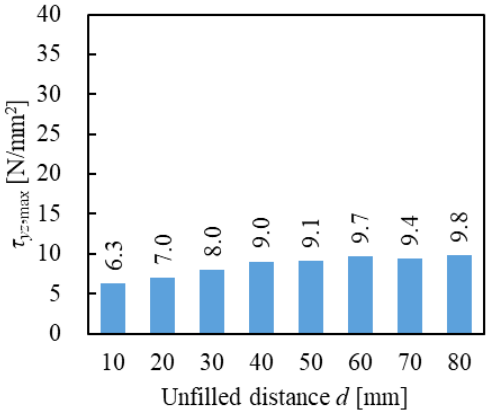

(c) Shear stress τ_{yz}

Figure 19. Variation of stress components with unfilled distance

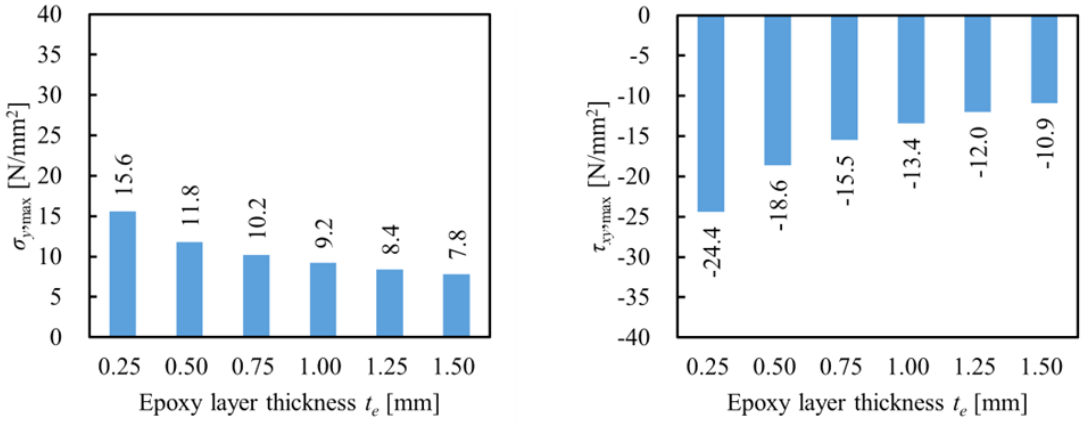

(a) Normal stress σ_y **(b) Shear stress τ_{xy}**

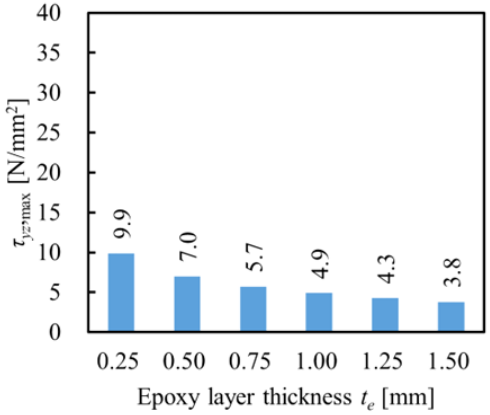

(c) Shear stress τ_{yz}

Figure 20. Variation of stress components with epoxy layer thickness

Analyzing the variations of different stress components as a function of the unfilled distance d in Figure 19 helps explain the trends observed in the maximum principal tensile stress $\sigma_{1,max}$ in Figure 17-c. When d is small, normal stress dominates, whereas shear stress becomes dominant as d increases. As shown in Figure 21, when d = 10 mm, the normal stress $\sigma_{y,max}$ is approximately 11.6 N/mm^2, while the shear stresses τ_{xy} and τ_{yz} at the corresponding locations are only approximately -8.2 N/mm^2 and 6.3 N/mm^2, respectively. As d increases, the normal stress gradually decreases, while the shear stress increases rapidly, causing the rapid increase in $\sigma_{1,max}$ in Figure 17-c. Beyond d = 40 mm, normal stress decreases rapidly, falling below 10 N/mm^2, while the shear stress increases slowly, exceeding 20 N/mm^2. At this point, the shear stress dominates and barely increases, resulting in the nearly stable $\sigma_{1,max}$ in Figure 17-c. This process can also be regarded as the process of epoxy aging due to oxidation. As the peripheral epoxy degrades, the unfilled distance increases. During this degradation, the epoxy's function gradually shifts from restricting normal relative displacement to primarily resisting shear displacement. Throughout the progression from d = 10 mm to d = 80 mm, σ_y remains low and steadily decreases, never exceeding 12 N/mm^2, while τ_{xy} stays high, increasing from -16.2 N/mm^2 to - 23.5 N/mm^2. Thus, the shear strength of the epoxy-bonded steel plates is a critical factor controlling the failure of epoxy-bonding-assisted welding. Furthermore, as shown in Figures 21 to 23, maximum stress always occurs at the outer edges of the epoxy layer; the inner epoxy, though initially lightly loaded, remains essential to provide sufficient bonding strength after outer-layer aging and ensure fatigue life improvement at the weld root.

As shown in Figure 20, the three stress components $\sigma_{y,max}$, $\tau_{xy,max}$ and $\tau_{yz,max}$ all decrease with the increase of t_e. Even under the condition where the stresses are highest (t_e = 0.25 mm), $\sigma_{y,max}$ and $\tau_{yz,max}$ are 15.6 N/mm^2 and 9.9 N/mm^2 respectively, which are generally below the typical strength limits of epoxy-bonded steel plates. However, $\tau_{xy,max}$ reaches -24.4 N/mm^2, exceeding the shear strength of commonly used epoxies. Therefore, a minimum thickness $t_e \geq 0.50$ mm is recommended to prevent epoxy failure. In this case, $\tau_{xy,max}$ remains below 20 N/mm^2, within the allowable range for most epoxy materials. Considering both the improvement in weld root fatigue life and construction feasibility, the epoxy thickness should not exceed 1.00 mm, which aligns with the findings in Section 4.2.2.

Assuming bonding-assisted welding with d = 20 mm and t_e = 0.50 mm, the weld root fatigue life can be increased by approximately 8.5 times relative to the original structure, comparable to the improvement achieved by Niwa et al. using tap bolts [14]. However, since bonding-assisted welding does not require drilling, it has less impact on the original structure, making it a highly promising solution for weld root fatigue mitigation.

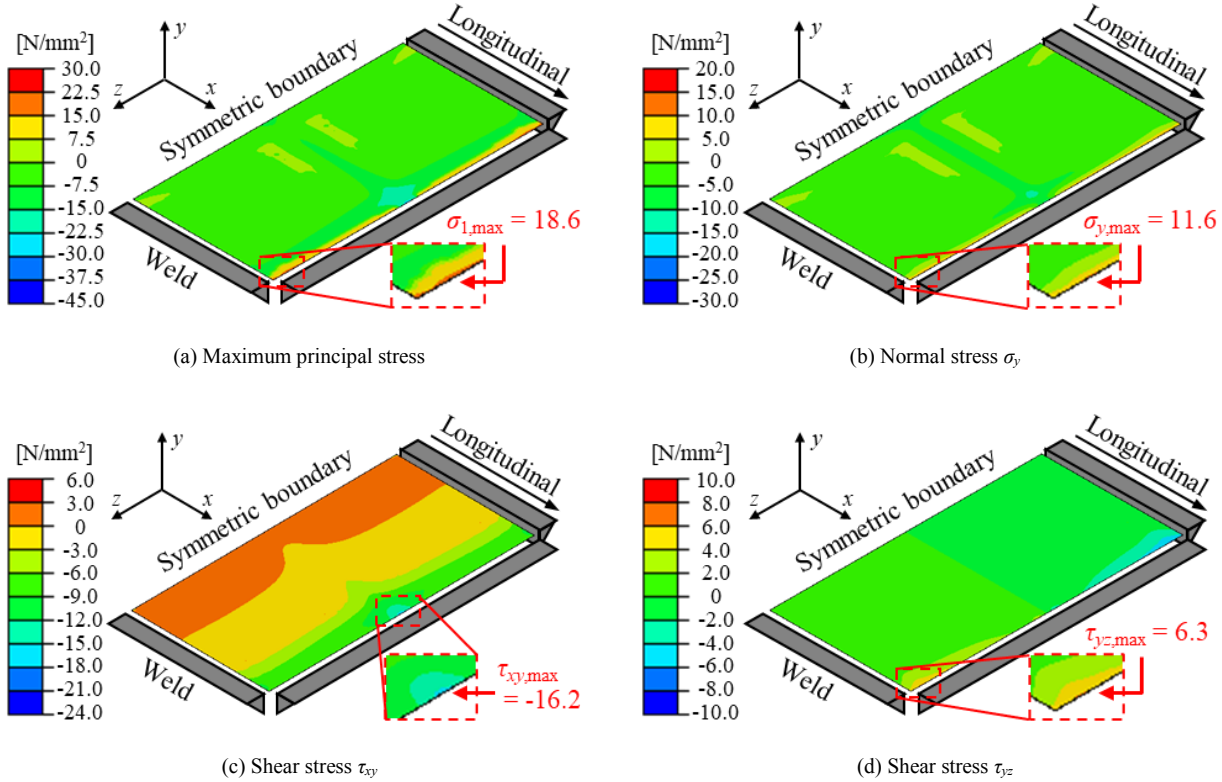

(a) Maximum principal stress

(b) Normal stress σ_y

(c) Shear stress τ_{xy}

(d) Shear stress τ_{yz}

Figure 21. Stress distribution of the epoxy layer (d = 10 mm, t_e = 0.50 mm)

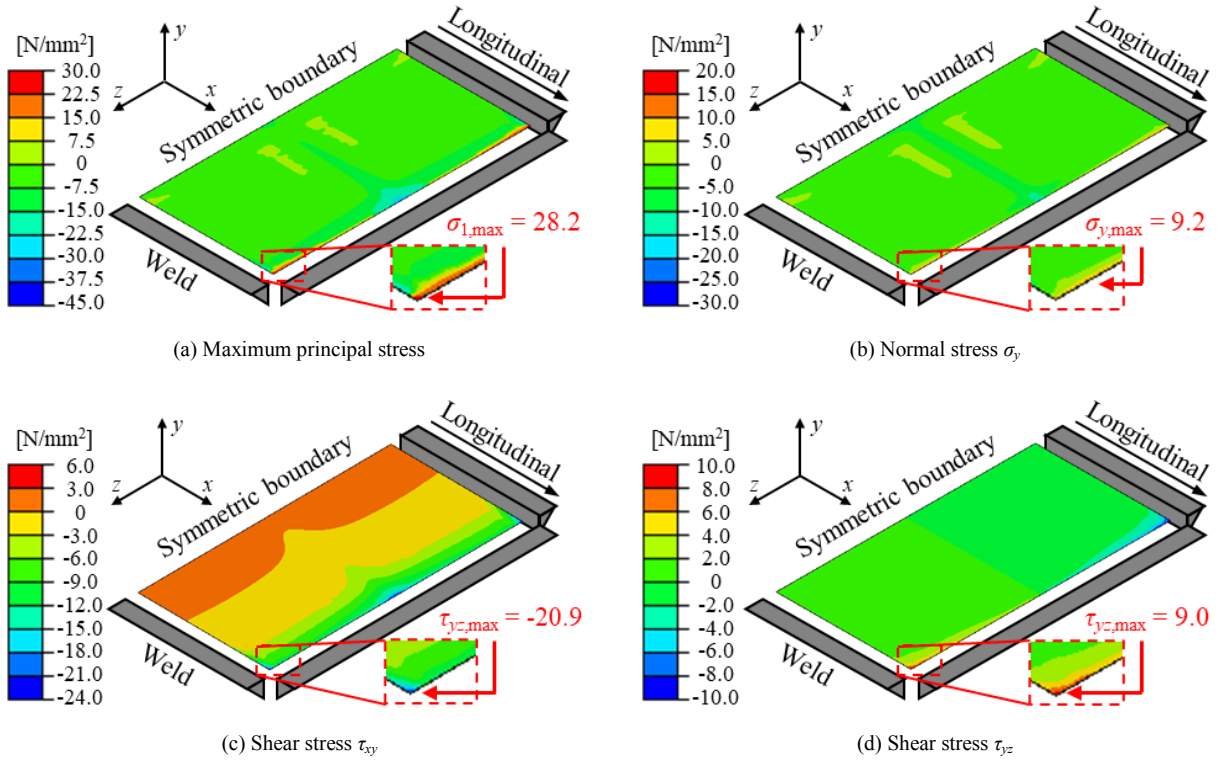

(a) Maximum principal stress (b) Normal stress σ_y

(c) Shear stress τ_{xy} (d) Shear stress τ_{yz}

Figure 22. Stress distribution of the epoxy layer (d = 40 mm, t_e = 0.50 mm)

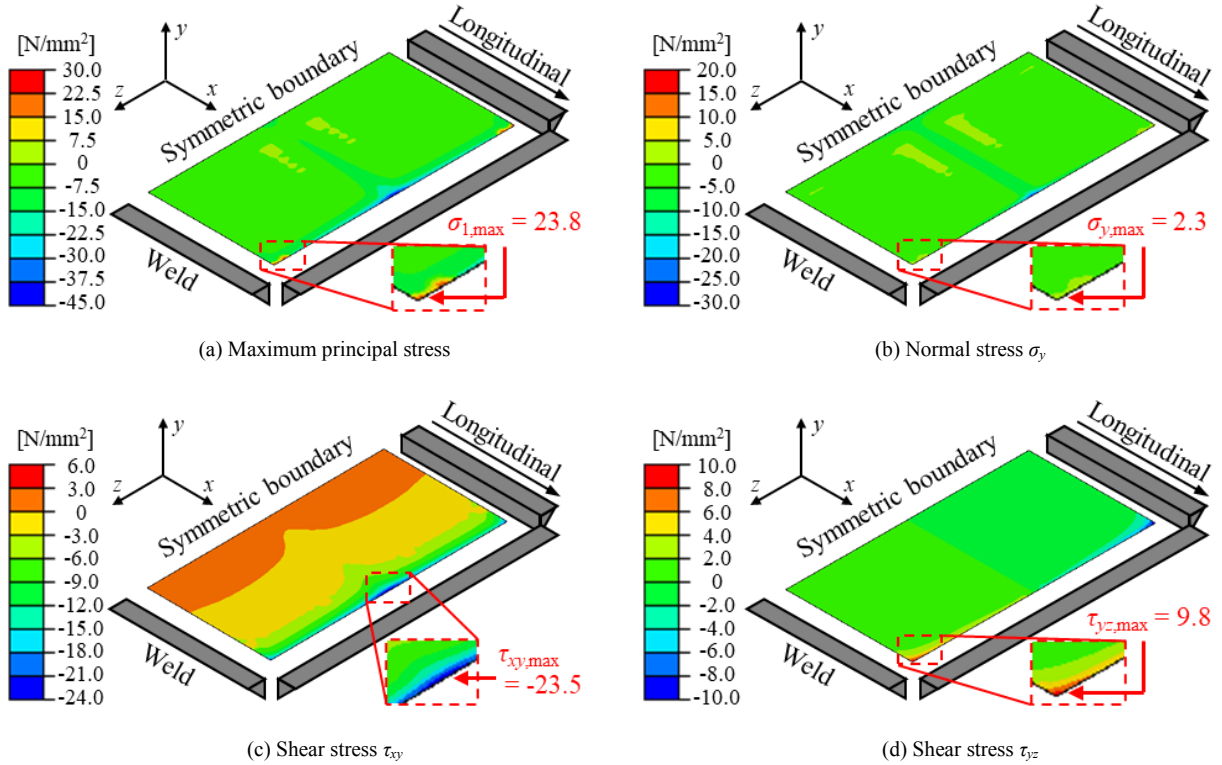

(a) Maximum principal stress (b) Normal stress σ_y

(c) Shear stress τ_{xy} (d) Shear stress τ_{yz}

Figure 23. Stress distribution of the epoxy layer (d = 80 mm, t_e = 0.50 mm)

5. Conclusions

This study compared five actual bridges to investigate the causes of fatigue cracks at the roots of fillet welds between the bottom flange and the sole plate of bridge supports. A series of parametric analyses was conducted through numerical simulations based on the Effective Notch Stress (ENS) method. Recommendations for enhancing the fatigue life of weld roots were proposed from both structural design and adhesive insertion perspectives. The main conclusions are as follows:

- The fillet weld root between the bottom flange and sole plate near the intermediate support of the continuous beam bridge is susceptible to high tensile stress, making it prone to fatigue cracking. This issue is more pronounced in bridges with large girders but fewer in number, and in those with a high live load ratio. For some bridges, the predicted fatigue life of the weld root is less than two million cycles.
- Increasing the fillet weld size significantly enhances the fatigue life of the weld root, whereas adjusting the sole plate thickness has limited effect. In cases with large sole plates, a hybrid connection using both bolts and welds is necessary. To optimize fatigue performance, bolts should be placed as close as possible to the weld root while satisfying clearance requirements.
- Bonding-assisted welding using epoxy insertion effectively improves the fatigue performance of weld roots, particularly in cases where structural design modifications alone are insufficient. For optimal performance and to avoid epoxy burning during welding, the unfilled distance from the epoxy layer to the weld root d should be between 15 mm and 40 mm. To balance fatigue enhancement and epoxy stress, the epoxy thickness t_e should be maintained between 0.50 mm and 1.00 mm. The shear strength of epoxy-bonded steel plates is the key factor in preventing bonding failure.

This study demonstrates the feasibility and effectiveness of applying bonding-assisted welding technology to bridge supports. However, further experimental and simulation studies are necessary to validate and refine the application of this technology.

6. Nomenclature

h_w	Height of web at support cross-section	t_w	Thickness of web at support cross-section
w_{b1}	Width of bottom flange at midspan cross-section	w_{b2}	Width of bottom flange at support cross-section
t_b	Thickness of bottom flange at support cross-section	l_s	Length of sole plate
w_s	Width of sole plate	t_s	Thickness of sole plate
l_w	Length of weld leg (fillet welds between bottom flange and sole plate)	$N_x(y)$, $N_y(x)$	Distributed normal loads in the x- and y-directions
$S_{xy}(y)$, $S_{yx}(x)$	Distributed shear loads in the x- and y-directions	k_1, k_2, k_3, k_4, σ_1, σ_2, τ_1, τ_2	Load constants obtained from the girder models
$\vec{d}$	Relative displacement between the paired nodes	$\vec{d}_A$	Displacement of the paired nodes on bottom flange
$\vec{d}_B$	Displacement of the paired nodes on sole plate	u_A, v_A, w_A	Displacement components of $\vec{d}_A$ in the x-, y- and z-directions
u_B, v_B, w_B	Displacement components of $\vec{d}_B$ in the x-, y- and z-directions	d	Unfilled distance from the weld root to the epoxy layer
t_e	Thickness of epoxy layer	$\sigma_{1,max}$	Maximum principal tensile stress in the epoxy layer
σ_y	Normal stress in the y-direction in the epoxy layer	τ_{xy}	Shear stress in the xy-plane in the epoxy layer
τ_{yz}	Shear stress in the yz-plane in the epoxy layer	$\sigma_{y,max}$	Maximum value of normal stress in the y-direction in the epoxy layer
$\tau_{xy,max}$	Maximum value of shear stress in the xy-plane in the epoxy layer	$\tau_{yz,max}$	Maximum value of shear stress in the yz-plane in the epoxy layer

7. Declarations

7.1. Author Contributions

Conceptualization, J.M. and M.H.; methodology, J.M. and F.J.; software, J.M. and F.J.; validation, J.M. and F.J.; formal analysis, J.M.; investigation, J.M. and F.J.; resources, M.H and Y.Q.; data curation, M.H and Y.Q.; writing—original draft preparation, J.M.; writing—review and editing, F.J., M.H and Y.Q.; visualization, J.M.; supervision, M.H.; project administration, F.J. and M.H.; funding acquisition, M.H. All authors have read and agreed to the published version of the manuscript.

7.2. Data Availability Statement

The data presented in this study are available on request from the corresponding author.

7.3. Funding

The authors received no financial support for the research, authorship, and/or publication of this article.

7.4. Conflicts of Interest

The authors declare no conflict of interest.

8. References

[1] Wright, W. J. (2012). Steel bridge design handbook: Bridge steels and their mechanical properties. No. FHWA-IF-12-052, Federal Highway Administration. Office of Bridge Technology, Washington, United States.

[2] Horvath, A., & Hendrickson, C. (1998). Steel versus Steel-Reinforced Concrete Bridges: Environmental Assessment. Journal of Infrastructure Systems, 4(3), 111–117. doi:10.1061/(asce)1076-0342(1998)4:3(111).

[3] Haghani, R., Al-Emrani, M., & Heshmati, M. (2012). Fatigue-prone details in steel bridges. Buildings, 2(4), 456–476. doi:10.3390/buildings2040456.

[4] Alencar, G., de Jesus, A., da Silva, J. G. S., & Calçada, R. (2019). Fatigue cracking of welded railway bridges: A review. Engineering Failure Analysis, 104, 154–176. doi:10.1016/j.engfailanal.2019.05.037.

[5] Fan, Y., Shuai, Y., Shuai, J., Zhang, T., Zhang, Y., Shi, L., & Shan, K. (2024). The effect of pipeline root weld microstructure on crack growth behaviour. Engineering Failure Analysis, 161, 108265. doi:10.1016/j.engfailanal.2024.108265.

[6] Hunter, R. N., Lang, A. S., & Carey, W. N. (1977). National Cooperative Highway Research Program Synthesis of Highway Practice 41: Bridge Bearings. Transportation Research Board, National Research Council, Washington, United States.

[7] Kaczinski, M., Oliver, K. (2022). Chapter 15 Bearing Design. Steel Bridge Design Handbook. American Institute of Steel Construction, Chicago, United States.

[8] Wang, Q., Okumatsu, T., Nakamura, S., Nishikawa, T., Wu, Q., & Chen, K. (2019). Fatigue Failure Analysis of Cracks near the Sole Plate of a Half-Through Steel-Arch Bridge. Journal of Bridge Engineering, 24(5), 5019004. doi:10.1061/(asce)be.1943-5592.0001380.

[9] Wang, W. J., Guo, J., Liu, Q. Y., Zhu, M. H., & Zhou, Z. R. (2009). Study on relationship between oblique fatigue crack and rail wear in curve track and prevention. Wear, 267(1–4), 540–544. doi:10.1016/j.wear.2008.12.100.

[10] Huang, C., Chen, T., Xia, Z., & Jiang, L. (2022). Numerical study of surface fatigue crack growth in steel plates repaired with CFRP. Engineering Structures, 268, 114743. doi:10.1016/j.engstruct.2022.114743.

[11] Ke, L., Li, Y., Chen, Z., Feng, Z., Yan, B., Zhu, F., & Yuan, P. (2023). Effect of microstructure on fatigue crack growth behavior of surface- and middle-layer materials of thick high-strength bridge steel plates. Fatigue & Fracture of Engineering Materials & Structures, 46(2), 485–500. doi:10.1111/ffe.13879.

[12] Ma, N., Feng, Z., Hiraoka, K., & Matsuzaki, T. (2024). Compressive residual stresses in LTT elongated bead welded in all positions for fatigue crack prevention of boxing fillet joints. Journal of Manufacturing Processes, 117, 82–94. doi:10.1016/j.jmapro.2024.02.059.

[13] Kühn, B., Lukic, M., Nussbaumer, A., Guenther, H. P., Helmerich, R., Herion, S., Kolstein, M.H.; Walbridge, S.; Androic, B.; Dijkstra, O.& Bucak, B. (2008). Assessment of existing steel structures-Recommendations for estimation of the remaining fatigue life. Office for Official Publications of the European Communities, Luxembourg, Luxembourg.

[14] Niwa, Y., Tateishi, K., Hanji, T., & Shimizu, M. (2024). Preventive Maintenance Measures Against Fatigue Cracks At Welded Joints of Sole Plates of Steel Bridges. Japanese Journal of JSCE, 80(5). doi:10.2208/jscejj.23-00234. (In Japanese).

[15] Hirohata, M. (2016). Static tensile strength characteristics of fillet welding lap joints assisted with bonding. Welding International, 30(1), 9–17. doi:10.1080/09507116.2014.921085.

[16] Mikihito, H., & Yoshito, I. (2018). Fatigue characteristics of patch plate joints by fillet welding assisted with bonding. Welding International, 32(4), 243–253. doi:10.1080/09507116.2017.1346217.

[17] Jiahao, M., Mikihito, H., Yifei, X., & Kyong-Ho, C. (2024). Fatigue performance of bonding-assisted fillet weld roots by inserting adhesive material. Fatigue & Fracture of Engineering Materials & Structures, 47(10), 3646–3657. doi:10.1111/ffe.14400.

[18] Mao, J., Hirohata, M., Jiang, F., & Hamasaka, D. (2026). Improving fatigue performance of fillet weld roots using soft metal insertion. Journal of Constructional Steel Research, 236, 110021. doi:10.1016/j.jcsr.2025.110021.

[19] Jiang, X., Lv, Z., Qiang, X., & Xu, Z. (2024). Fatigue performance of root-to-throat cracks repaired by bonding steel: experimental and numerical investigations. Journal of Constructional Steel Research, 212, 108296. doi:10.1016/j.jcsr.2023.108296.

[20] Radaj, D., Sonsino, C. M., & Fricke, W. (2006). Fatigue assessment of welded joints by local approaches. Woodhead Publishing Limited, Sawston, United Kingdom. doi:10.1533/9781845691882.

[21] Fricke, W. (2013). IIW guideline for the assessment of weld root fatigue. Welding in the World, 57(6), 753–791. doi:10.1007/s40194-013-0066-y.

[22] Iqbal, M., Karuppanan, S., Perumal, V., Ovinis, M., & Iqbal, M. (2025). Development of Novel Surrogate Models for Stress Concentration Factors in Composite Reinforced Tubular KT-Joints. Civil Engineering Journal (Iran), 11(4), 1458–1475. doi:10.28991/CEJ-2025-011-04-012.

[23] Vu, H. H., Vu, Q. A., & Pham, C. H. (2024). Global Buckling Strength of Girts with Inner Flange in Compression. Civil Engineering Journal, 10(11), 3531–3541. doi:10.28991/CEJ-2024-010-11-05.

[24] Zhang, G. (2012). Method of effective stress for fatigue: Part I - A general theory. International Journal of Fatigue, 37, 17–23. doi:10.1016/j.ijfatigue.2011.09.018.

[25] Fricke, W., Kahl, A., & Paetzold, H. (2006). Fatigue assessment of root cracking of fillet welds subject to throat bending using the structural stress approach. Welding in the World, 50(7–8), 64–74. doi:10.1007/BF03266538.

[26] Fricke, W. (2007). Round-robin study on stress analysis for the effective notch stress approach. Welding in the World, 51(3–4), 68–79. doi:10.1007/BF03266562.

[27] Sonsino, C. M., Fricke, W., De Bruyne, F., Hoppe, A., Ahmadi, A., & Zhang, G. (2012). Notch stress concepts for the fatigue assessment of welded joints - Background and applications. International Journal of Fatigue, 34(1), 2–16. doi:10.1016/j.ijfatigue.2010.04.011.

[28] Hobbacher, A. F. (2016). Recommendations for Fatigue Design of Welded Joints and Components. IIW Collection, Springer International Publishing, Cham, Switzerland. doi:10.1007/978-3-319-23757-2.

[29] Yoon, D. Y., Yoo, C. H., & Lee, S. C. (2004). On the behavior of sole plates in steel girders. Thin-Walled Structures, 42(1), 59–77. doi:10.1016/S0263-8231(03)00123-X.

[30] AASHTO. (2020). LRFD Bridge Design Specifications (9th Ed.). American Association of State Highway and Transportation Officials (AASHTO), Washington, United States.

[31] JTG D60-2015. (2015). General Specifications for Design of Highway Bridges and Culverts. Ministry of Transport of the People's Republic of China, Beijing, China. (In Chinese).

[32] TB 10002-2017. (2017). Code for Design on Railway Bridge and Culvert. (2017). Beijing: National Railway Administration of the People's Republic of China, Beijing, China. (in Chinese).

[33] Japan Road Association. (2017). Specifications for Highway Bridges. Japan Road Association, Tokyo, Japan . (In Japanese).

[34] Tao, G., & Xia, Z. (2007). Mean stress/strain effect on fatigue behavior of an epoxy resin. International Journal of Fatigue, 29(12), 2180–2190. doi:10.1016/j.ijfatigue.2006.12.009.

Appendix I: Mesh Convergence

This study employed the ENS method to analyze weld root fatigue stresses. The reference radius of the notch r_{ref}, = 1 mm, and the mesh size around the notch perimeter in all models was approximately 0.2 mm. To verify mesh convergence, additional models with a finer mesh size of 0.1 mm were constructed for comparison. Using the original designs of the five bridges as examples, the results are shown in Figure A1. The difference between the results obtained with the two mesh sizes was less than 6%, indicating that the models have achieved satisfactory convergence.

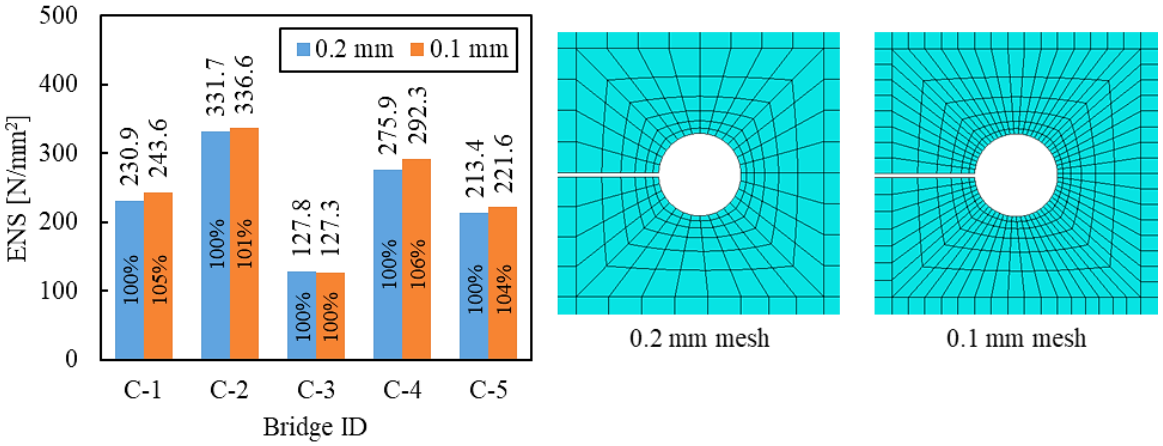

Figure A1. Verification of mesh convergence